ACS APPLIED MATERIALS & INTERFACES

Research Article

www.acsami.org

# Design of LVFFARK and LVFFARK-Functionalized Nanoparticles for Inhibiting Amyloid β-Protein Fibrillation and Cytotoxicity

Neng Xiong,[†] Xiao-Yan Dong,[†] Jie Zheng,[‡] Fu-Feng Liu,*[,†] and Yan Sun*[,†]

[†]Department of Biochemical Engineering and Key Laboratory of Systems Bioengineering of the Ministry of Education, School of Chemical Engineering and Technology, Tianjin University, Tianjin 300072, China

[‡]Department of Chemical and Biomolecular Engineering, The University of Akron, Akron, Ohio 44325, United States

Supporting Information

**ABSTRACT:** Aggregation of amyloid β-protein (Aβ) into amyloid oligomers and fibrils is pathologically linked to Alzheimer's disease (AD). Hence, the inhibition of Aβ aggregation is essential for the prevention and treatment of AD, but the development of potent agents capable of inhibiting Aβ fibrillogenesis has posed significant challenges. Herein, we designed Ac-LVFFARK-$NH_2$ (LK7) by incorporating two positively charged residues, R and K, into the central hydrophobic fragment of Aβ17−21 (LVFFA) and examined its inhibitory effect on Aβ42 aggregation and cytotoxicity by extensive physical, biophysical, and biological analyses. LK7 was observed to inhibit Aβ42 fibrillogenesis in a dose-dependent manner, but its strong self-assembly characteristic also resulted in high cytotoxicity. In order to prevent the cytotoxicity that resulted from the self-assembly of LK7, the peptide was then conjugated to the surface of poly(lactic-*co*-glycolic acid) (PLGA) nanoparticles (NPs) to fabricate a nanosized inhibitor, LK7@PLGA-NPs. It was found that LK7@PLGA-NPs had little cytotoxicity because the self-assembly of the LK7 conjugated on the NPs was completely inhibited. Moreover, the NPs-based inhibitor showed remarkable inhibitory capability against Aβ42 aggregation and significantly alleviated its cytotoxicity at a low LK7@PLGA-NPs concentration of 20 μg/mL. At the same peptide concentration, free LK7 showed little inhibitory effect. It is considered that several synergetic effects contributed to the strong inhibitory ability of LK7@PLGA-NPs, including the enhanced interactions between Aβ42 and LK7@PLGA-NPs brought on by inhibiting LK7 self-assembly, restricting conformational changes of Aβ42, and thus redirecting Aβ42 aggregation into unstructured, off-pathway aggregates. The working mechanisms of the inhibitory effects of LK7 and LK7@PLGA-NPs on Aβ42 aggregation were proposed based on experimental observations. This work provides new insights into the design and development of potent NPs-based inhibitors against Aβ aggregation and cytotoxicity.

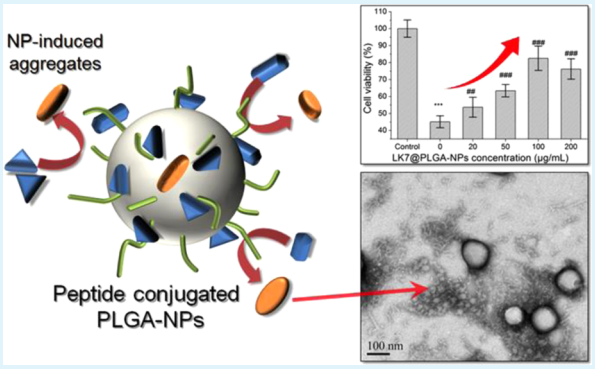


**KEYWORDS:** *Alzheimer's disease, protein aggregation, amyloid β-protein, peptide inhibitor, self-assembly, nanoparticle*

## 1. INTRODUCTION

Alzheimer's disease (AD), the most common form of senile dementia, is pathologically featured by the accumulation of intracellular neurofibrillary tangles formed by tau proteins and extracellular senile plagues by amyloid β-proteins (Aβ) in the patient brain.[1,2] Aβ containing 39−43 residues is normally produced by sequential cleavage of the amyloid precursor protein (APP) by both β- and γ-secretases.[3] Upon cleavage, Aβ40 and Aβ42 are the two most common isoforms, where Aβ42 is considered as the most toxic form while Aβ40 as the most abundant form. Many studies have proven that the aggregation of Aβ into amyloid fibrils containing characteristic cross-β-sheet structure in the brain of AD patients is tightly linked to the pathogenesis of AD.[4] Moreover, it is generally accepted that soluble Aβ oligomers or protofibrils are the most toxic species, responsible for neuron dysfunction and death. Therefore, inhibition of Aβ aggregation at the very early stage could be a promising treatment for preventing or delaying the onset of AD.

Significant efforts and progress have been made to develop different amyloid inhibitors, including small organic compounds,[5−10] peptides and peptide mimetics,[11] antibodies,[12] and nanoparticles (NPs).[13] They were found to be capable of binding to Aβ, preventing Aβ polymerization into fibrils, and/or reducing cell toxicity in vitro.[14] Among them, some peptides and peptide derivatives were found to inhibit Aβ aggregation, and most peptide-based inhibitors were derived from the Aβ sequence, particularly from the central hydrophobic sequence Aβ16−20 (KLVFF)[15] and C-terminal fragment Aβ39−42 (VVIA).[16] Due to highly homologous sequences between Aβ and its fragments, it is not surprising that Aβ fragmental

Received: August 7, 2014
Accepted: February 20, 2015
Published: February 20, 2015





DOI: 10.1021/acsami.5b00915
ACS Appl. Mater. Interfaces 2015, 7, 5650−5662

inhibitors could interact with a similar sequence or structure of Aβ to interfere with Aβ aggregation.

NPs have attracted substantial attention in the therapeutics of AD due to their unique structural superiority, high stability, ease of surface functionalization and modification, and ready ability to cross the blood−brain barrier (BBB).[17,18] Several NPs, including PEGylated NPs,[19] polymeric NPs,[20−22] $Fe_3O_4$ NPs,[23] gold NPs,[24−28] and fullerene NPs,[29] have been identified for their inhibitory ability to prevent amyloid fibrillation. The inhibition performance of NPs is largely controlled by their intrinsic structural and surface properties (i.e., size and shape, net charge and its distribution, and surface hydrophobicity), which in turn control the interactions between Aβ and NPs to regulate Aβ aggregation.[30−34] Liao et al.[25] have reported that the negatively charged gold NPs inhibited Aβ fibrillation and reduced Aβ40-induced cell toxicity. Moreover, some anti-amyloid molecules such as curcumin,[35−38] EGCG,[39] and peptides,[40] were conjugated with NPs to further enhance the inhibitory performance of NPs. These NPs functionalized by anti-amyloid molecules can generally help to improve binding affinity and specificity between anti-amyloid inhibitors and Aβ,[41] penetration ability to cross the BBB,[36] and solubility.[37] These advantages offer more feasibility and flexibility to develop effective NP-based inhibitors for AD treatment.

Poly(lactic-*co*-glycolic acid) (PLGA) NP is a US FDA-approved NP for drug delivery, owing to its excellent biocompatibility and biodegradability.[42] In this study, peptide-functionalized PLGA-NPs were developed as an Aβ aggregation inhibitor. First, a novel heptapeptide, Ac-LVFFARK-$NH_2$ (LK7), was rationally designed and its anti-amyloid capacity was examined. Despite enhanced anti-amyloid capacity as compared to its precursor peptide LVFFA, the strong self-aggregation character and the corresponding toxicity would hinder its further practical applications. In order to overcome the above limits, LK7 peptides were conjugated to the surface of PLGA-NPs to obtain a nanosized inhibitor, LK7@PLGA-NPs. Then, the inhibitory effects of LK7@PLGA-NPs on Aβ42 aggregation and cytotoxicity were extensively examined by using thioflavin-T (ThT), transmission electron microscopy (TEM), dynamic light scattering (DLS), circular dichroism (CD), and cell viability assay. Finally, we explored the molecular mechanisms of the inhibitory effects of LK7 and LK7@PLGA-NPs on Aβ42 aggregation.

## 2. EXPERIMENTAL SECTION

**2.1. Materials.** PLGA (lactide:glycolide 50/50, $M_w$ ~17 000 Da), poly(vinyl alcohol) (PVA, $M_w$ 9000−10 000 Da, 80% hydrolyzed), dimethyl sulfoxide (DMSO), hexafluoro-2-propanol (HFIP), and ThT were purchased from Sigma-Aldrich (St. Louis, MO). Both Aβ42 and heptapeptide LK7 (>95% purity) were purchased from GL Biochem (Shanghai, China). Dulbecco's modified Eagle's medium (DMEM) and fetal bovine serum were obtained from Gibco Invitrogen (Grand Island, NY). All other chemicals were the highest purity available from local sources.

**2.2. Aβ42 Preparation.** Aβ42 was prepared as described in the literature.[43] Aβ42 was first dissolved in HFIP solutions to a final concentration of 1.0 mg/mL. The solution was in quiescence at least 2 h and then sonicated for 30 min to destroy the pre-existing Aβ aggregates. Thereafter, the solution was centrifuged for 30 min at 15 000*g* and 4 °C to remove the existing Aβ aggregates. About the top 75% of supernatant was collected and the solvent was removed by vacuum freeze-drying overnight. Before use, Aβ was dissolved in 10.0 mM NaOH, centrifuged for 20 min at 16 000*g* and 4 °C to remove the aggregates, and then diluted with 10.0 mM phosphate buffer solution (PBS) (100 mM NaCl, pH 7.4) to a final concentration of 40 μM.

**2.3. Synthesis and Characterization of PLGA-NPs.** PLGA-NPs were produced using an emulsion solvent evaporation method.[44] Briefly, 100 mg of PLGA was dissolved in 10.0 mL of acetonitrile. Then, the solution was added dropwise to 20.0 mL of PVA solution (2% w/v) and kept stirring at 800 rpm for 3 h. After evaporation of acetonitrile, PLGA-NPs were collected by centrifugation at 12 000*g* for 45 min. Then, PLGA-NPs were washed three times using deionized water. Finally, PLGA-NPs were suspended in PBS buffer solutions for further use. The structural properties (e.g., morphology, size, and ζ-potential) of PLGA-NPs were determined by TEM and dynamic light scattering (DLS) experiments.

**2.4. Conjugation of LK7 to PLGA-NPs.** Before use, PLGA-NPs were suspended in deionized water at a concentration of 5 mg/mL. The NPs were activated in the presence of 0.4 M *N*-(3-(dimethylamino)propyl)-*N*′-ethylcarbodiimide hydrochloride and 0.1 M *N*-hydroxysuccinimide at 25 °C for 1 h with gently stirring. Then, LK7 was added to a final concentration of 0.5 mg/mL, and the mixture was mixed well and incubated for 4 h at room temperature with gentle stirring. To remove excess reactants and precipitates, the resulting PLGA-NPs were dialyzed for 3 d and collected successively by 10 kDa ultrafiltration membrane and 0.45 μM filtration membrane. The obtained LK7@PLGA-NPs were resuspended in PBS buffer solution and deionized water, respectively. LK7@PLGA-NPs were dissolved in 50% DMSO-$d_6$ and 50% $CDCl_3$, and their chemical structure was validated by $^1$H NMR.

**2.5. Thioflavin T (ThT) Fluorescence Assay.** Aβ42 was dissolved in DMSO and centrifuged at 16 000*g* for 20 min to remove the aggregates. Then, the obtained Aβ42 solution was immediately diluted to 40 μM with 10 mM PBS buffer solution (pH 7.4, NaCl 100 mM). Thereafter, Aβ42 solutions were incubated at 37 °C with various concentrations of inhibitors, and continuous shaking at 150 rpm was employed. Aliquots of incubation solutions at different time points were then diluted 20 times into ThT solution (25 μM ThT in 25 mM PB buffer, pH 6.0). ThT fluorescence was measured by a fluorescence spectrophotometer (LS-55, PerkinElmer) at 25 °C. The slit width was 5 nm. ThT emission was monitored at 480 nm with the excitation at 440 nm. The fluorescence intensity of solution without Aβ42 was subtracted as background from each read with Aβ42. Three measurements were performed and the data were averaged.

**2.6. Transmission Electron Microscopy.** The morphology of Aβ42 aggregates with or without inhibitors was studied using TEM. The incubation solutions were diluted to appropriate concentrations, dropped onto Formvar carbon-coated copper grids (400-mesh), and air-dried for 2 min. Then the samples were stained with 2% phosphotungstic acid for 5 min, and excess solution was removed by filter paper. Finally, the stained samples were examined and photographed using a JEM-100CXII TEM system (JEOL Inc., Tokyo, Japan) with an accelerating voltage of 100 kV.

**2.7. Dynamic Light Scattering.** The size distribution of NPs and NP−Aβ42 aggregates were measured using a Malvern Nanosizer 2000. The NP solutions and the incubation solutions of Aβ42 with NPs were diluted to the appropriate concentrations, transferred into a clear disposable zeta cell, and measured at 25 °C. Three measurements of each sample were employed at a single backscatter angle of 173°.

**2.8. Circular Dichroism (CD) Spectroscopy.** The CD spectra of 40 μM Aβ42 monomer solution in the absence and presence of inhibitors were recorded using a J-810 circular dichroism spectropolarimeter (JASCO). A quartz cell with 1 mm path length was used for far-UV (190−260 nm) measurements with 1 nm bandwidth at a scan speed of 100 nm/min. The background signal of solution without Aβ42 was subtracted from the sample spectra. All CD spectra were the average of three consecutive scans for each sample.

**2.9. Cytotoxicity Assay.** In vitro cytotoxicity assays were performed using two neuronal cell lines (i.e., SH-SY5Y and PC12) which have been commonly used as in vitro cellular models for AD. Two different kinds of cytotoxicity test methods [i.e., 3-(4,5-dimethylthiazol-2-yl)-2,5-diphenyltetrazolium bromide (MTT) and lactate dehydrogenase (LDH) leakage assays] were used to determine the cell viability.[45] The MTT method is a colorimetric assay for assessing cell viability.[46] Instead, the LDH leakage assay, a well-known


DOI: 10.1021/acsami.5b00915
ACS Appl. Mater. Interfaces 2015, 7, 5650−5662

indicator of cell membrane integrity and cell viability, is based on the measurement of lactate dehydrogenase released in the extracellular medium upon cell death and lysis.[47] SH-SY5Y cells were cultured in DMEM/F-12 medium supplemented with 20% fetal bovine serum (FBS) and 2 mM L-glutamine. PC12 cells were cultured in DMEM supplemented with 10% FBS. In MTT assay, the cells were plated at a density of 5000 cells/well in 96-well plates with 90 $\mu$L of fresh medium. After incubation for 24 h, the aged A$\beta$ aggregates with different concentrations of inhibitors (10 $\mu$L each well) were added into the plates, and the cells were incubated for another 48 h. After that, 10 $\mu$L of MTT solutions (6.0 mg/L) was added into each well, and the plates were incubated for another 4 h. The culture medium was removed by centrifugation, and the precipitated cells were lysed using DMSO. After the purple crystals were dissolved completely, the cell viability was calculated from the absorbance signals measured by a plate reader (Tecan) at 570 nm wavelength. The wells containing medium only were subtracted as the background from each reading. The cell viability data were normalized as a percentage of the control group without A$\beta$42 and inhibitors.

In the LDH leakage assay, cell death was quantitatively assessed by measuring the release of LDH. Briefly, after 24 h seeding, the culture medium was replaced with FBS-free medium, and then A$\beta$42 and inhibitors-modified A$\beta$42 (inhibitors were coincubated with A$\beta$42 monomers at 37 °C for 24 h) were added into the cells. After treatment for 48 h, the LDH leakage assay was performed. Prior to assay, the cells were incubated with 1% (v/v) Triton X-100 in FBS-free medium at 37 °C for 1 h to obtain a representative maximal LDH release as the positive control with 100% cytotoxicity. Extracellular LDH leakage was evaluated using an assay kit (Roche Diagnostics) according to the manufacturer's instructions. Briefly, cells in 96-well plates were centrifuged at 250$g$ for 10 min, 50 $\mu$L of culture supernatant was collected from each well, and 50 $\mu$L of reaction buffer supplied in the kit was then added. The leakage of LDH was assessed at a test wavelength of 490 nm with 630 nm as the reference wavelength after mixing for 30 min at room temperature. The cytotoxicity and LDH release data, representative of at least three independent experiments carried out with different cell culture preparations, are presented as mean ± SEM. Analysis of variance was carried out for statistical comparisons using $t$-test, and $p < 0.05$ or less was considered to be statistically significant.

## 3. RESULTS AND DISCUSSION

**3.1. Design of Heptapeptide LK7 and Examination of Its Inhibitory Effect on A$\beta$42 Fibrillation.** Some fragments of full-length A$\beta$40/42 (i.e., KLVFF and LVFFA) were found to bind to A$\beta$ and are often used as a basic element for designing new peptide inhibitors against A$\beta$ aggregation.[48,49] The pentapeptide LVFFA can bind to the similar $\beta$-sheet region of A$\beta$ via hydrophobic interactions and hydrogen bonds, thus preventing A$\beta$ fibrillation (Figure 1);[50] however, LVFFA is a weak inhibitor. Soto et al.[51] found that when incubating 1 $\mu$g/$\mu$L A$\beta$42 with a 10-fold molar excess of LVFFA, ~92% fibrils were still formed. In wild-type A$\beta$ sequence, two negatively charged residues, E and D, are next to LVFFA (i.e., LVFFAED) near the N-terminal $\beta$-sheet region. To improve potential binding affinity between LVFFA-based inhibitor and A$\beta$, two positively charged residues, R and K, were purposely incorporated into LVFFA, yielding a new heptapeptide inhibitor, LVFFARK (LK7). We expect that not only the high sequence similarity of LK7 would promote its binding with the corresponding region of the target A$\beta$ but also the RK in LK7 would bind more strongly to the target ED residues in A$\beta$ via enhanced electrostatic interactions. Both effects will lead to a better peptide inhibitor against A$\beta$ aggregation.

As a proof-of-concept, the inhibitory effect of LK7 on A$\beta$42 aggregation was first examined using ThT fluorescence and TEM (Figure 2). Figure 2a showed the aggregation kinetics of

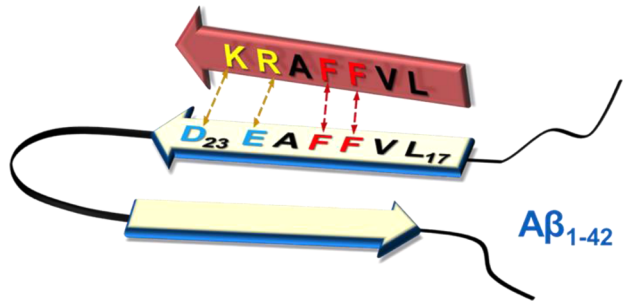


**Figure 1.** Rational design of peptide inhibitor LK7 and its interaction with the fibril form of A$\beta$42. The amino acids of LK7 and A$\beta$42 are signified by single-letter code. Red, dashed arrows represent hydrophobic interactions between hydrophobic residues, while yellow, dashed arrows represent the electrostatic interactions between charged residues.

amyloid fibril formation at different molar ratios of LK7:A$\beta$42 using the time-dependent ThT fluorescence. When incubating 40 $\mu$M A$\beta$42 alone at 37 °C for 72 h, the ThT fluorescence profile showed an almost negligible lag phase, a fast growth phase within 12 h, and a steady equilibrium phase after 12 h. TEM images taken from the same samples of ThT assays also confirmed that pure A$\beta$ formed short fibrils at 24 h and long-branched, thick fibrils at 72 h (Figure 2b). To evaluate LK7 inhibitory activity against A$\beta$ aggregation, we used the maximum intensity of ThT fluorescence obtained from pure A$\beta$—measured for a total of formation of amyloid fibrils—to normalize other ThT profiles. Overall, upon incubation of LK7 with freshly prepared A$\beta$42 solution (40 $\mu$M) at different molar ratios of LK7:A$\beta$ (0.2:1, 0.5:1, 1:1, 2:1, and 5:1), ThT profiles showed that LK7 inhibited A$\beta$ aggregation at substochiometric concentrations in a dose-dependent manner. At the low concentration of LK7 (8 $\mu$M), LK7 did not exhibit any inhibitory effect on A$\beta$ (40 $\mu$M) aggregation, as evidenced by the almost identical ThT curve of LK7/A$\beta$ compared to that of pure A$\beta$. When LK7 concentration increased to 20 $\mu$M (i.e., LK7:A$\beta$ = 0.5:1), the ThT intensity of the LK7/A$\beta$ mixture was decreased by ~29% at 24 h and 48% at 72 h, relative to that of pure A$\beta$. When the LK7:A$\beta$ ratio was further increased to 1:1, a stronger inhibition on A$\beta$ fibrillation formation was observed, with the final ThT intensity being reduced by ~69%. TEM images of the samples prepared with the equimolar LK7 only showed a few amorphous aggregates at 24 h (Figure 2b). When incubation time was extended to 72 h, small amorphous aggregates still remained and they did not convert into any amyloid-like fibrils (Figure 2b). As compared to LK7, the coincubation of equimolar LVFFA/A$\beta$ mixture only reduced the final ThT intensity by 5% under the same conditions (Figure S1, Supporting Information), suggesting that LK7 has much stronger ability to inhibit A$\beta$ amyloid formation than its precursor LVFFA.

It is interesting to observe that as LK7 concentrations further increased to 80 and 200 $\mu$M, the final ThT intensities of LK7:A$\beta$ mixtures at 2:1 and 5:1 molar ratios achieved 42% and 51% relative to that of pure A$\beta$, respectively, both of which were higher than the 31% ThT intensity at LK7:A$\beta$ of 1:1. Increased ThT intensities indicated that more A$\beta$ fibrils were formed, consistent with TEM images showing a large amount of fibrils (Figure S2, Supporting Information). We should note that in all tested LK7:A$\beta$ mixtures containing the same amount of A$\beta$ (40 $\mu$M), any increase in final ThT intensity may result


DOI: 10.1021/acsami.5b00915
ACS Appl. Mater. Interfaces 2015, 7, 5650−5662

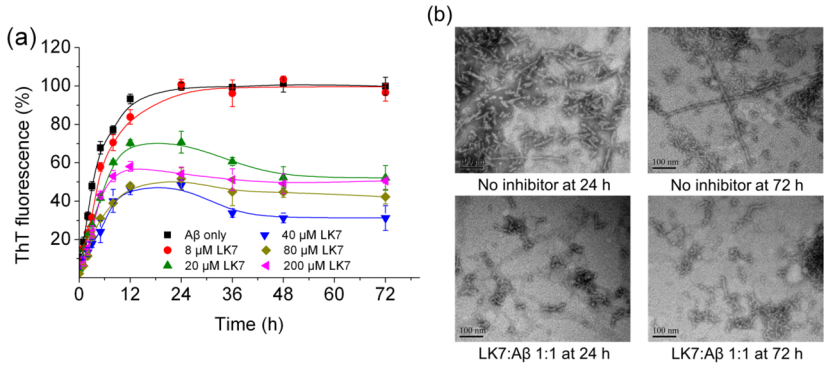


**Figure 2.** Inhibition effects of LK7 on A$\beta$42 fibrillation. (a) Time-dependent ThT fluorescence changes for A$\beta$42 incubated with different concentrations of LK7. ThT fluorescence of A$\beta$42 aggregates without LK7 was defined as 100%. (b) TEM images of the morphologies of A$\beta$42 aggregates when coincubating without and with equimolar concentration of LK7 after 24 and 72 h of incubation. A$\beta$42 concentration was 40 $\mu$M.

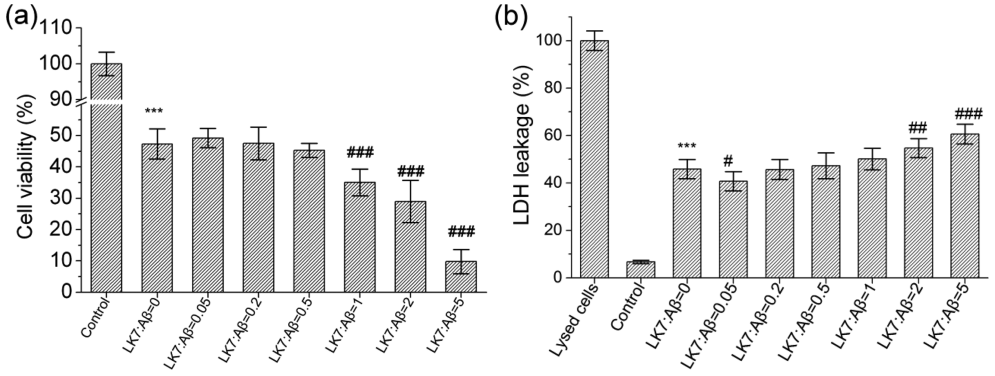


**Figure 3.** Inhibitory effect of LK7 on A$\beta$42-induced cytotoxicity using (a) MTT assay and (b) LDH leakage assay. A$\beta$ concentration was 40 $\mu$M. In the MTT assay, cell viability for treatment with PBS buffer alone was set to 100%. In the LDH leakage assay, the cells were incubated with 1% (v/v) Triton X-100 in FBS-free medium at 37 °C for 1 h to obtain a representative maximal LDH release as the positive control with 100% cytotoxicity. ***$p < 0.001$, compared to control groups. $^{\#}p < 0.05$, $^{\#\#}p < 0.01$, $^{\#\#\#}p < 0.001$, compared to the A$\beta$42-treated group (LK7:A$\beta$ = 0).

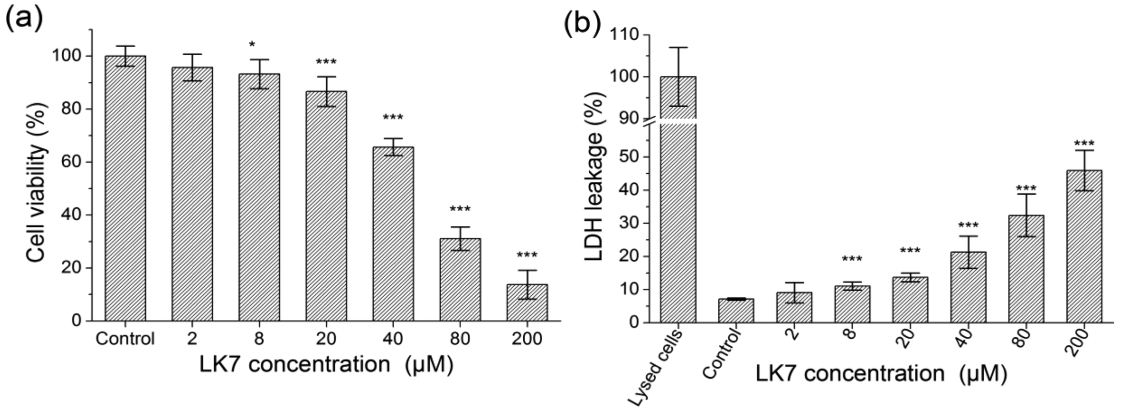


**Figure 4.** Cytotoxicity of SH-SY5Y induced by LK7 aggregates using (a) MTT assay and (b) LDH leakage assay. In the MTT assay, the cell viability treated with PBS buffer alone was set to 100%. In the LDH leakage assay, the cells were incubated with 1% (v/v) Triton X-100 in FBS-free medium at 37 °C for 1 h to obtain a representative maximal LDH release as the positive control with 100% cytotoxicity. *$p < 0.05$, ***$p < 0.001$, compared to control groups.

from either A$\beta$ fibrils alone or LK7 fibrils. To test this hypothesis, when incubating LK7 (40 $\mu$M and 200 $\mu$M) alone at 37 °C for 72 h, we observed that LK7 can aggregate into long and thick amyloid-like fibrils with morphologies similar to that of typical A$\beta$ fibrils (Figure S3, Supporting Information). Interestingly, Figure S4 (Supporting Information) shows that different from A$\beta$ fibrils, which excited significant ThT signals, LK7 fibrils produced almost negligible ThT signals at all LK7 concentrations tested from 8 to 200 $\mu$M. When the LK7-to-A$\beta$42 concentration ratio was 2:1 or 5:1, the more LK7 that self-assembled into fibrils, the less free LK7 in solution that could interact with A$\beta$42 and, consequently, the more A$\beta$42 fibrils that formed, as evidenced by enhanced ThT intensities. Therefore, the loss of inhibitory ability of LK7 at high concentrations could be attributed to its self-assembly ability. It appears that there exist optimal concentrations of LK7 to achieve highly effective inhibition of A$\beta$ fibrillation.


DOI: 10.1021/acsami.5b00915
ACS Appl. Mater. Interfaces 2015, 7, 5650−5662

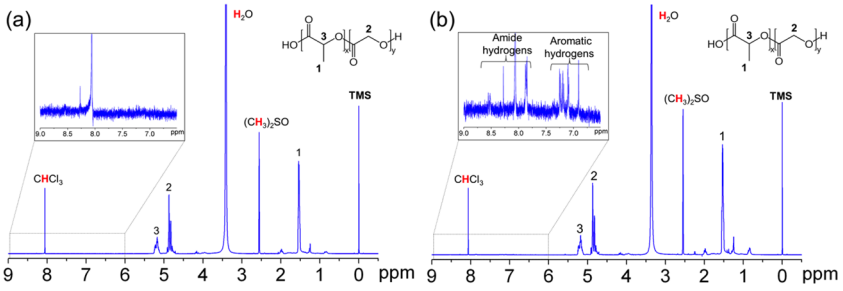


**Figure 5.** $^1$H NMR spectra [in 50% $CDCl_3$ and 50% $(CD_3)_2SO$] of (a) PLGA-NPs and (b) LK7@PLGA-NPs.

In order to determine whether LK7 is able to modulate A$\beta$-induced cell death, two neuronal cell lines of SH-SY5Y and PC12 were used to examine the effect of LK7 on the cytotoxicity of A$\beta$ aggregates. Figure 3a shows the inhibitory effect of LK7 on A$\beta$42-induced cytotoxicity against SH-SY5Y cells using the MTT assay. In the absence of LK7, upon 24 h of incubation of pure A$\beta$42 (40 $\mu$M) with SH-SY5Y cells, A$\beta$ caused a significant reduction in cell viability of ~45% relative to the untreated control (Figure 3a). In the presence of 2 $\mu$M LK7, cell viability increased slightly to ~49%. However, as LK7 concentrations increased from 8 to 20 $\mu$M, cell viability decreased slightly to ~47%. This toxic effect became even more pronounced at high concentrations of LK7. Upon coincubation of 80 $\mu$M LK7 with A$\beta$42 (i.e., LK7:A$\beta$ = 2:1), cell viability decreased to ~29% (Figure 3a). Especially, as LK7 concentrations increased to 200 $\mu$M (i.e., LK7:A$\beta$ = 5:1), cell viability was only about 10% (Figure 3a). The LDH assay showed a trend similar to that of SH-SY5Y viability in the MTT assay; i.e., cell viability decreased with LK7 concentrations (Figure 3b). Consistently, similar cell toxicity results were obtained using both assays for PC12 cells (Figure S5, Supporting Information). A combination of aggregate and toxicity data appears to suggest that inhibition of A$\beta$42 fibrillation by LK7 leads to some amorphous aggregates (Figure 2b), which in turn induce higher toxicity to cells than pure A$\beta$ aggregates.

It is also equally important to determine whether LK7 aggregates are toxic to cells. Thus, we conducted cell viability experiments to test the cytotoxic effect of LK7 aggregates alone. Figures 4 and S6 (Supporting Information) show the concentration effect of LK7 aggregates (2−200 $\mu$M) on cytotoxicity of both SH-SY5Y and PC12 cells. Clearly, LK7 aggregates were cytotoxic to both cells in a dose-dependent manner [Figures 4 and S6 (Supporting Information)]. In Figure 4a, treatment of SH-SY5Y cells with 80 $\mu$M LK7 reduced cell viability to ~31%, and further increase of LK7 concentration to 200 $\mu$M led to a significant reduction in cell viability of ~14%. Similar cell toxicity results were obtained using LDH leakage assays (Figure 4b). Similar concentration dependence of LK7 on PC12 cell toxicity was obtained (Figure S6, Supporting Information), consistent with SH-SY5Y results. Considering the self-aggregation feature of LK7 as discussed above (Figure S3, Supporting Information), we concluded that the self-assembly of LK7 not only greatly compromised its inhibitory ability against A$\beta$ aggregation but also induced strong cytotoxicity to cells. Thus, LK7 cannot be directly used as a candidate inhibitor for AD therapy.

**3.2. Synthesis and Characterization of LK7-Conjugated PLGA-NPs.** The aforementioned data have shown that LK7 exhibits dose-dependent inhibitory ability to prevent A$\beta$ aggregation; however, LK7 also possesses a strong self-assembly to form amyloid-like fibrils, which induce strong cytotoxicity to cells at high concentrations. To remedy the toxicity issue induced by LK7 aggregates, we proposed to conjugate LK7 onto PLGA-NPs, which would eliminate the self-assembly of LK7 and thus suppress its self-assembly induced toxicity.

Herein, PLGA-NPs, approved by US FDA, were selected as the scaffolds to conjugate LK7 to improve its potential therapeutic efficacy. Figure S7 (Supporting Information) illustrates the synthesis process for LK7@PLGA-NPs. First, PLGA-NPs were synthesized using the emulsion evaporation method as reported in a previous study.[52] LK7 was anchored to PLGA-NPs via the conventional EDC/NHS reaction between the $\varepsilon$-amino group of K residues in LK7 and carboxyl groups on the surface of PLGA-NPs (Figure S7, Supporting Information). The conjugation of LK7 onto PLGA-NPs was confirmed by $^1$H NMR (Figure 5). The $^1$H NMR spectrum of PLGA-NPs revealed three typical proton peaks for methyl groups at 1.54 ppm, methylene groups at 4.85 ppm, and methanetriyl groups at 5.22 ppm, indicated by 1, 2, and 3 in Figure 5. For LK7@PLGA-NPs, the peaks of aromatic protons at 7.00−7.50 ppm corresponded to FF residues of LK7 (Figure 5b). The peaks of amide and guanidine protons at 7.80−8.50 ppm corresponded to all of the residues and the R residue of LK7, respectively. Comparing the peak area of aromatic groups of LK7 on LK7@PLGA-NPs with that of PLGA-NPs suggests a grafting rate of ~25% of LK7 on the surface of PLGA-NPs. On the basis of this grafting ratio, the concentrations of LK7 anchored onto NPs in 20, 100, and 200 $\mu$g/mL LK7@PLGA-NPs were estimated to be 0.29, 1.45, and 2.90 $\mu$M, respectively. Moreover, $\zeta$-potential is used as a reaction indicator by the comparison between PLGA-NPs and LK7@PLGA-NPs. We observed that the $\zeta$-potential was decreased from −31.07 mV for PLGA-NPs to −10.04 mV for LK7@PLGA-NPs (Table 1). The reduction of $\zeta$-potential was attributed to the introduction of the positively charged R and K residues of LK7. Both NMR and $\zeta$-potential data confirmed that LK7 was successfully conjugated onto PLGA-NPs.

**Table 1. $\zeta$-Potential and Size Distributions of PLGA-NPs and LK7@PLGA-NPs**

| nanoparticle | size (nm) | PDI | $\zeta$-potential (mV) |
|---|---|---|---|
| PLGA-NPs | 150.07 ± 0.06 | 0.04 ± 0.02 | −31.07 ± 0.25 |
| LK7@PLGA-NPs | 161.00 ± 1.51 | 0.21 ± 0.01 | −10.04 ± 0.29 |

The structural parameters of PLGA-NPs and LK7@PLGA-NPs were characterized by DLS and SEM. A SEM image showed that PLGA-NPs alone had monodispersion and homogeneous spherical structures, with an average diameter between 90 and 120 nm (Figure S8, Supporting Information). DLS data showed an average size of ~150 nm for PLGA-NPs


DOI: 10.1021/acsami.5b00915
ACS Appl. Mater. Interfaces 2015, 7, 5650−5662

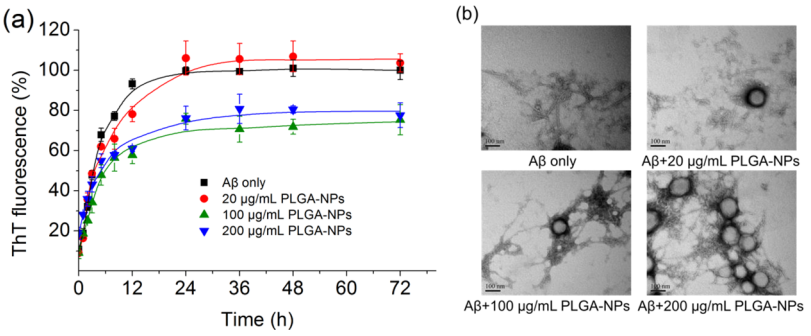


**Figure 6.** Inhibitory effect of PLGA-NPs on A$\beta$42 fibrillation. (a) ThT fluorescence of A$\beta$42 incubated in the absence and presence of various concentrations of PLGA-NPs. ThT fluorescence of A$\beta$42 aggregates without PLGA-NPs was defined as 100%. (b) TEM images of the morphologies of A$\beta$ aggregates coincubated with different concentrations of PLGA-NPs after 24 h. A$\beta$42 concentration was 40 $\mu$M.

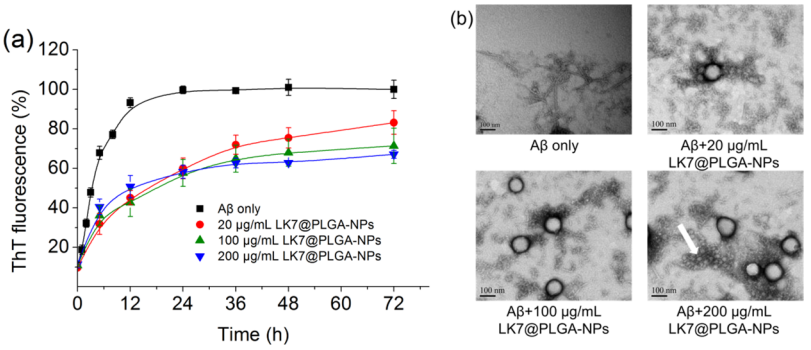


**Figure 7.** LK7@PLGA-NPs inhibited A$\beta$42 fibrillation. (a) ThT fluorescence of A$\beta$42 incubated in the absence and presence of various concentrations of LK7@PLGA-NPs. ThT fluorescence of A$\beta$42 aggregates without LK7@PLGA-NPs was defined as 100%. (b) TEM images of the morphologies of A$\beta$ aggregates coincubated with 20−200 $\mu$g/mL LK7@PLGA-NPs after 24 h. The small amorphous aggregates are indicated by a white arrow. A$\beta$42 concentration was 40 $\mu$M.

(Table 1). The difference in NPs size as measured by SEM and DLS was because DLS considered the hydration layer of the NPs, while SEM did not. Upon conjugating LK7 (a small molecular mass of 0.9 kDa) on the surface of PLGA-NPs, the average size of LK7@PLGA-NPs slightly increased to ~161 nm by DLS (Table 1). Both PLGA-NPs and LK7@PLGA-NPs showed long stability, retaining their sizes and $\zeta$-potential in PBS solution for 7 days.

**3.3. Inhibitory Effect of LK7@PLGA-NPs on A$\beta$42 Fibrillation.** ThT fluorescence, TEM, and DLS were used to probe the inhibitory effect of LK7@PLGA-NPs and its control PLGA-NPs on A$\beta$42 fibrillation. The ThT profiles in Figure 6a show that PLGA-NPs had almost no inhibitory effect on A$\beta$42 aggregation at a low concentration (20 $\mu$g/mL), as evidenced by the almost identical ThT profile compared to that of pure A$\beta$42. However, when the concentration of PLGA-NPs was further increased to 100−200 $\mu$g/mL, stronger inhibition on A$\beta$ fibril formation was observed, with the final ThT intensities being decreased by 22%. TEM images in Figure 6b show that regardless of PLGA-NPs concentrations, PLGA-NPs were able to capture and adsorb A$\beta$42 aggregates, as indicated by the contrasting dark regions around PLGA-NPs. The presence of PLGA-NPs of different concentrations showed no obvious effects on the morphology of A$\beta$ aggregates, with some short A$\beta$42 fibrils being observed by TEM.

DLS data showed that pure PLGA-NPs were able to well maintain their initial hydrodynamic size around 150 nm (Figure S9a, Supporting Information), with undetectable size change within 24 h. Upon coincubation of PLGA-NPs (100 $\mu$g/mL) with A$\beta$42 (180 $\mu$g/mL), it is apparent from the DLS results that the size distribution in A$\beta$42 and PLGA-NPs mixtures increased over time (Figure S9a, Supporting Information). The initial peak around 150 nm was dramatically decreased at 6 h and then completely disappeared at 24 h, while simultaneously producing a new large peak around ~1000 nm. This indicates that PLGA-NPs can indeed adsorb A$\beta$ species to form A$\beta$−PLGA-NPs complexes, consistent with the observation using TEM in Figure 6b.

LK7@PLGA-NPs at all concentrations tested significantly inhibited A$\beta$42 fibrillation (Figure 7a). Specifically, the presence of LK7@PLGA-NPs reduced the ThT intensities by ~40% at 20−200 $\mu$g/mL at 12 h, as well as by 39.7% at 20 $\mu$g/mL, 42.1% at 100 $\mu$g/mL, and 41.5% at 200 $\mu$g/mL at 24 h. It appeared that LK7@PLGA-NPs were more effective at inhibiting A$\beta$42 aggregation in the early stage. Particularly, free LK7 (i.e., 0.29 $\mu$M) and control PLGA-NPs (i.e., 20 $\mu$g/mL) exhibited almost no inhibitory effect, but LK7@PLGA-NPs at the same concentration indeed showed significant inhibitory capability against A$\beta$ fibrillation. So, the enhanced inhibitory ability of LK7@PLGA-NPs was attributed to the presence of LK7 exposed at the surface of PLGA-NPs. Similar to PLGA-NPs, TEM images showed that LK7@PLGA-NPs could still retain the adsorbed A$\beta$42 on their surfaces without disassociation (Figure 7b). DLS data showed a similar increase in size distribution for an A$\beta$42 and LK7@PLGA-NPs mixture over time, but the presence of LK7@PLGA-NPs led to a rapid disappearance of the initial 150 nm peak at 6 h (Figure S9b, Supporting Information). Different from PLGA-NPs, LK7@PLGA-NPs induced A$\beta$ to form many small amorphous aggregates (as indicated by a white arrow in Figure 7b). So,


DOI: 10.1021/acsami.5b00915
ACS Appl. Mater. Interfaces 2015, 7, 5650−5662

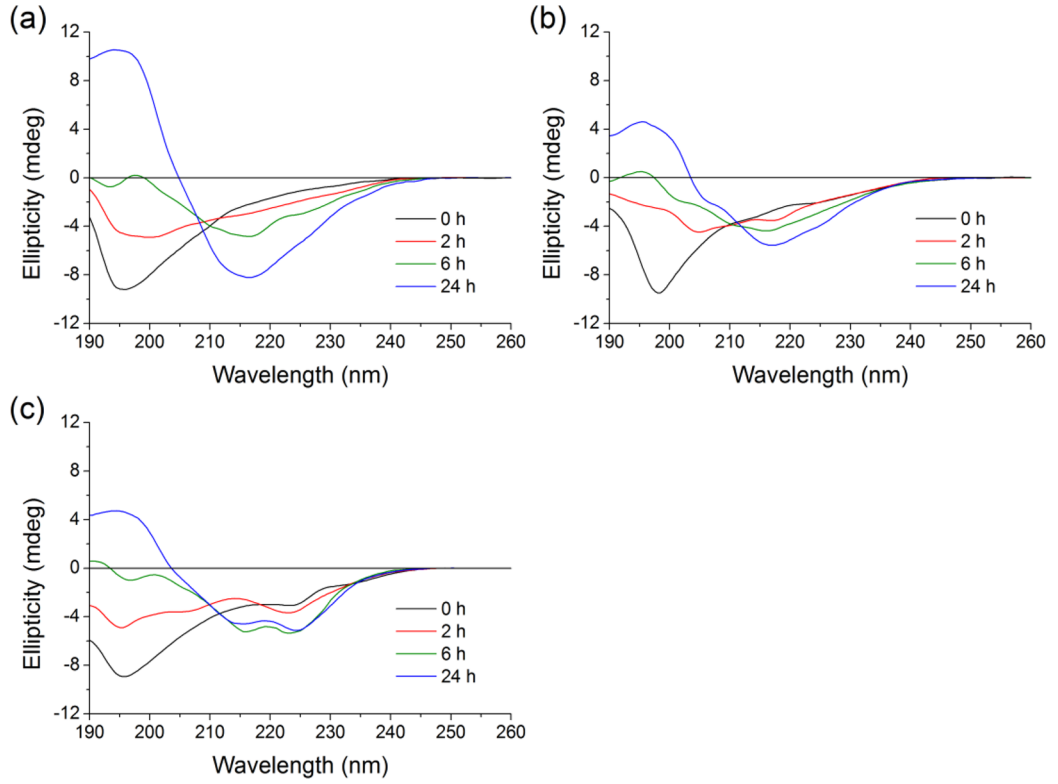


**Figure 8.** Far-UV circular dichroism spectra of A$\beta$42 incubated in the absence and presence of different concentrations of NPs at 0, 2, 6, and 24 h: (a) A$\beta$42 alone, (b) A$\beta$42 incubated with 100 $\mu$g/mL PLGA-NPs, and (c) A$\beta$42 incubated with 100 $\mu$g/mL LK7@PLGA-NPs.

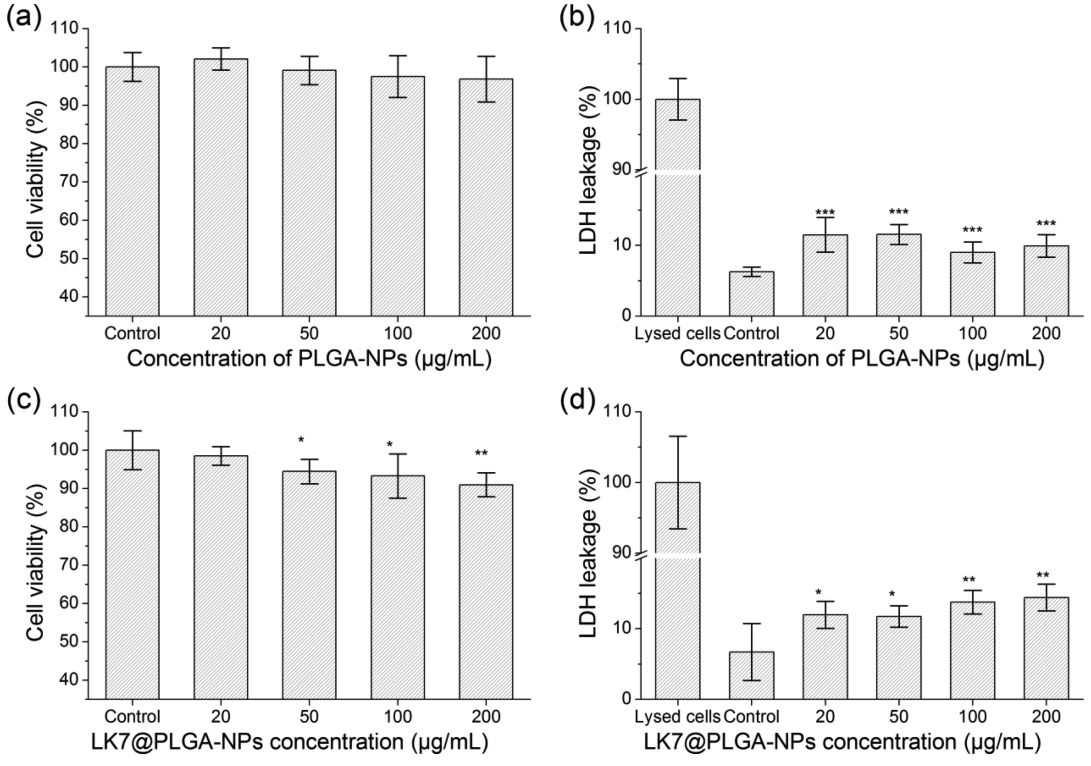


**Figure 9.** Cytotoxicity of SH-SY5Y induced by (a and b) PLGA-NPs and (c and d) LK7@PLGA-NPs. Cell viability was estimated by (a and c) MTT and (b and d) LDH leakage assays. In the MTT assay, the cell viability treated with PBS buffer only was set to 100%. In the LDH leakage assay, the cells were incubated with 1% (V/V) Triton X-100 in FBS-free medium at 37 °C for 1 h to obtain a representative maximal LDH release as the positive control with 100% cytotoxicity. *$p$ < 0.05, **$p$ < 0.01, ***$p$ < 0.001, compared to control groups.

conjugation of LK7 onto PLGA-NPs could greatly enhance binding affinity between LK7@PLGA-NPs and A$\beta$ species, which made LK7@PLGA-NPs prevent the A$\beta$ fibrillation and facilitate the formation of amorphous aggregates.



DOI: 10.1021/acsami.5b00915
ACS Appl. Mater. Interfaces 2015, 7, 5650−5662

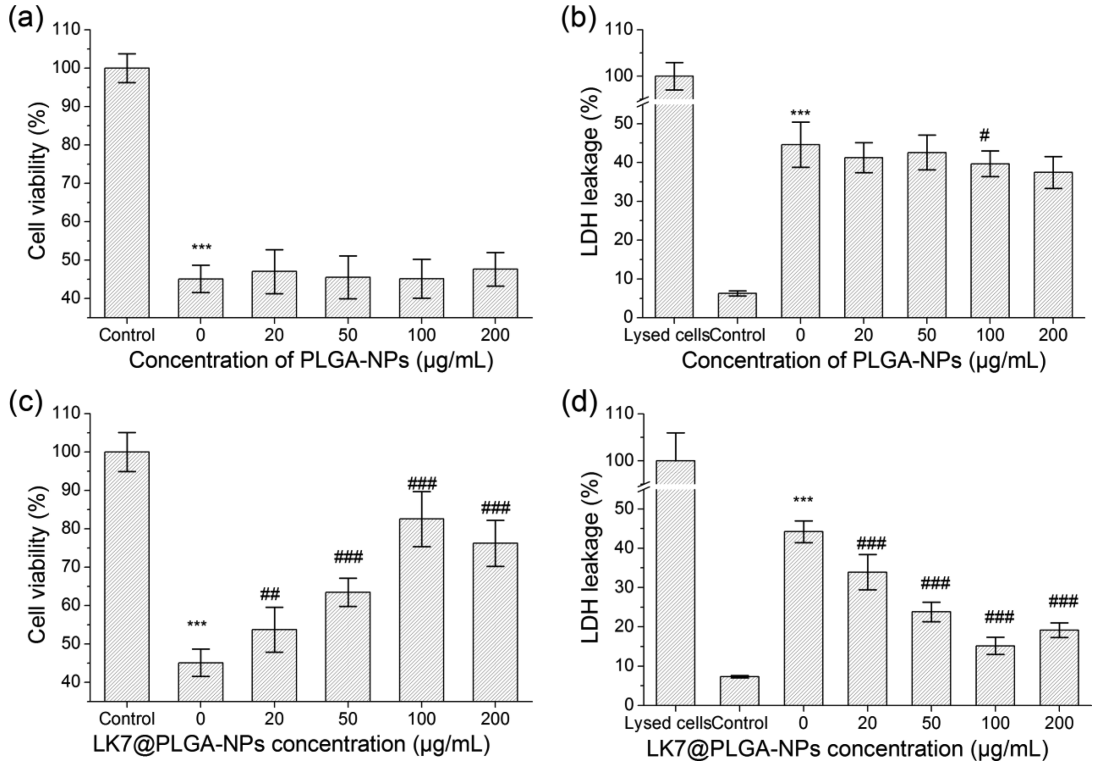


**Figure 10.** Inhibitory effect of (a and b) PLGA-NPs and (c and d) LK7@PLGA-NPs on A$\beta$42-induced cytotoxicity toward SH-SY5Y cells. A$\beta$42 concentration was 40 $\mu$M. Cell viability was estimated by (a and c) MTT and (b and d) LDH assays. In the MTT assay, the cell viability with PBS buffer only was set to 100%. In the LDH leakage assay, the cells were incubated with 1% (v/v) Triton X-100 in FBS-free medium at 37 °C for 1 h to obtain a representative maximal LDH release as the positive control with 100% cytotoxicity. ***$p < 0.001$, compared to control groups. $^{\#}p < 0.05$, $^{\#\#}p < 0.01$, $^{\#\#\#}p < 0.001$, compared to the A$\beta$42-treated group.

**3.4. Effect of LK7@PLGA-NPs on the Secondary Structure of A$\beta$42.** To gain insight into the effects of NPs on the conformational transition of A$\beta$42 upon aggregation, far-UV CD spectroscopy was applied to monitor the secondary structure of A$\beta$42 over time (Figure 8). As a control, the initial secondary structure of A$\beta$42 was a random coil with a representative negative minimum of ~195 nm (Figure 8a). Upon protein aggregation, this peak diminished gradually. After 24 h, a positive peak and a negative valley appeared at around 195 and 215 nm, respectively (Figure 8a). This indicates that A$\beta$42 converted from its initial random coil to a $\beta$-sheet structure, consistent with previous studies.[53]

The presence of 100 $\mu$g/mL PLGA-NPs in A$\beta$ solution showed a similar conformational transition of A$\beta$42 from initial random coils to $\beta$-sheet structures (Figure 8b). But the final content of $\beta$-structures was less than that of A$\beta$ alone at 24 h (Figure 8b). That is, PLGA-NPs can notably delay the onset of the conformational transition of A$\beta$42. Figure 8c shows the CD spectra of A$\beta$ incubated in the presence of 100 $\mu$g/mL LK7@PLGA-NPs. It is evidenced that the conformational changes of A$\beta$42 were partially suppressed, as indicated by two broad negative minimums around 215 and 225 nm at 24 h (Figure 8c). These two distinct bands corresponded to a mixture of $\alpha$-helix and $\beta$-sheet structures.[54] Figure S10 (Supporting Information) shows the CD spectra of control PLGA-NPs and LK7@PLGA-NPs without A$\beta$42 at 0 and 24 h. It can be seen that these NPs had almost no effect on the CD spectra. It is concluded that LK7@PLGA-NPs partially inhibited the conformational transition of A$\beta$42 from random coils to $\beta$-sheets, which indicates the inhibitory effects of LK7@PLGA-NPs on A$\beta$ aggregation.

**3.5. Effect of LK7@PLGA-NPs on A$\beta$42-Induced Cytotoxicity.** The concentration effects of LK7@PLGA-NPs and its control PLGA-NPs on cytotoxicity in the absence and presence of A$\beta$ were evaluated using both SH-SY5Y and PC12 cell lines (Figure 9). MTT assays showed that without A$\beta$42, bare PLGA-NPs at concentrations from 20 to 200 $\mu$g/mL presented almost no cytotoxicity to both cells, as evidenced by the ~100% cell viability, the same as the untreated control [Figures 9a and S11a (Supporting Information)]. Consistently, the LDH leakage assay showed only ~10% LDH leakage when both cells were treated by 20−200 $\mu$g/mL PLGA-NPs, which was slightly higher than that in the control group [Figures 9b and S11b (Supporting Information]. Therefore, PLGA-NPs demonstrated their noncytotoxicity to cells, consistent with previous results that PLGA-NPs are biocompatible and nontoxic materials.[55,56] When incorporating LK7 to nontoxic PLGA-NPs, MTT assays also showed that LK7@PLGA-NPs alone exerted an almost noncytotoxic effect on SH-SY5Y cells at a low concentration of 20 $\mu$g/mL (i.e., ~99% of cell viability). However, at high concentrations of LK7@PLGA-NPs (50−200 $\mu$g/mL), the cell survival rate was decreased by ~9% (Figure 9c), suggesting relatively weak toxicity to SH-SY5Y cells. In parallel, the LDH leakage assay showed that the cell survival rate was reduced slightly from 88% to 85% at all LK7@PLGA-NPs concentrations tested, 20−200 $\mu$g/mL (Figure 9d). Similar toxicity results were obtained for PC12 cells (Figures S11c,d, Supporting Information). Overall, LK7@PLGA-NPs were demonstrated to be very weakly cytotoxic to cells.

Next, we examined whether LK7@PLGA-NPs and their control PLGA-NPs can protect the two neuronal cells from A$\beta$-induced cytotoxicity using both MTT and LDH assays. When


DOI: 10.1021/acsami.5b00915
ACS Appl. Mater. Interfaces 2015, 7, 5650−5662

mixing A$\beta$42 with PLGA-NPs in the cultured cells, it can be seen clearly in Figure 10a that PLGA-NPs at all concentrations tested led to cell viability of ~47%, comparable to 45% cell viability with A$\beta$42 alone. This indicates that despite of nontoxic nature of PLGA-NPs, PLGA-NPs also cannot effectively protect the cells from A$\beta$42-induced cell toxicity at various concentrations. Similar results were obtained using an alternative LDH leakage assay (Figure 10b) and PC12 cells (Figures S12a,b, Supporting Information). In contrast, when LK7@PLGA-NPs of different concentrations were added to A$\beta$42 solution, they all protected SH-SY5Y cells from A$\beta$-induced apoptosis to some extent, and the protection effect was dose-dependent. As compared to an A$\beta$-induced cell viability of 45.1%, LK7@PLGA-NPs cell viability rates were improved by 8.7% at 20 $\mu$g/mL, 18.4% at 50 $\mu$g/mL, 37.5% at 100 $\mu$g/mL, and 31.1% at 200 $\mu$g/mL (Figure 10c). Figure 10d shows the cell viability of SH-SY5Y in the presence of A$\beta$42 using the LDH leakage assay. Consistently, cell viability was improved greatly with the increase of LK7@PLGA-NPs concentrations from 20 to 100 $\mu$g/mL, which is consistent with the MTT results. Similar inhibitory effects of LK7@PLGA-NPs on A$\beta$42-induced cytotoxicity were also observed for PC12 cells using both MTT (Figure S12c, Supporting Information) and LDH leakage assays (Figure S12d, Supporting Information). Taken together, these results demonstrate that LK7@PLGA-NPs are promising and effective inhibitors that can reduce A$\beta$42-induced cytotoxicity to both SH-SY5Y and PC12 cells.

**3.6. Mechanistic Models for the Inhibitory Action of LK7 and LK7@PLGA-NPs.** On the basis of our collective data, we proposed mechanistic models to elucidate the inhibitory effects of LK7 and LK7@PLGA-NPs on A$\beta$42 aggregation (Figure 11). A$\beta$ amyloid formation is a multiple self-assembly process, involving assembly of unfolded *monomers* to *oligomers* (structured aggregates exhibiting $\beta$-sheet structure) to *protofibrils* (elongated aggregates ~2−5 nm in diameter) to *fibrils* (entwined protofilaments up to 10 $\mu$m in length and 10 nm in width),[57] as shown in Figure 11a. This self-assembly process also requires different A$\beta$ species to undergo complex conformational transition and reorganization between species. LK7 is likely to interact with its homologous sequence of the parent A$\beta$ and mediate the aggregation of A$\beta$ (Figure 11b). Due to their high sequence similarity and concentration-dependent self-assembly properties (Figure S3, Supporting Information), both LK7 and A$\beta$ may preserve some common structural recognition motifs for interacting with each other. Moreover, the presence of two positively charged residues, R and K, in LK7 provides additional electrostatic interactions between LK7 and A$\beta$. All these effects lead to the enhanced LK7−A$\beta$ interactions, which competitively reduce A$\beta$−A$\beta$ interactions and thus inhibit A$\beta$ aggregation. However, the self-assembling ability of LK7 also causes strong cytotoxicity to SH-SY5Y (Figure 4) and PC12 cells (Figure S6, Supporting Information). It is well-known that the peptide inhibitors suffer from poor proteolytic stability. In order to improve peptide stability, it is often necessary to introduce D-amino acids[58] and *N*-methyl groups[59,60] to the sequence of LK7. Moreover, LK7 can be easily transformed into peptidomimetics using "*retro−inverso*" peptides[61] and cyclic peptides.[62] Another common strategy to improve peptide stability is to conjugate peptides with NPs, because the conformational flexibility was constricted after the peptides were coupled with NPs. Moreover, the electrical double layer formed on the surface of NPs also helps

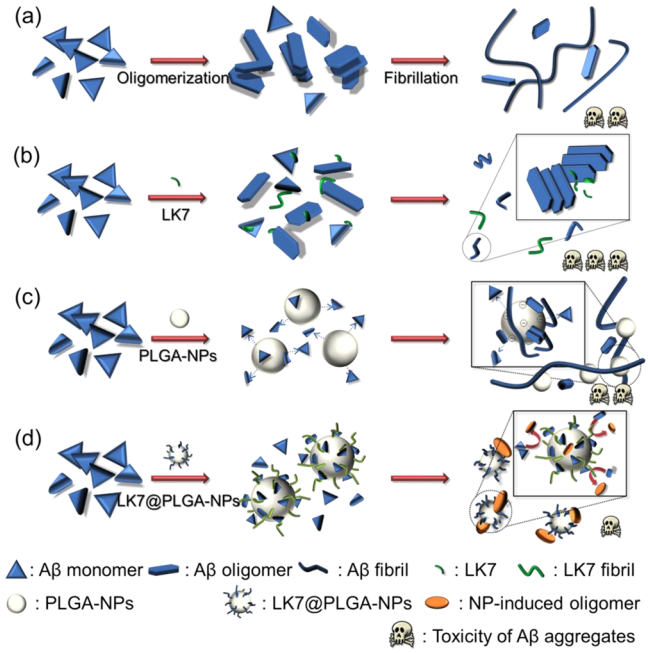


**Figure 11.** Schematic of A$\beta$42 fibrillogenesis influenced by different inhibitors. (a) A$\beta$42 monomers aggregate into mature fibrils through a well-known nucleation−polymerization mechanism, responsible for the cell cytotoxicity caused by A$\beta$ aggregates. (b) LK7 can inhibit A$\beta$42 fibrillation, but its inhibitory ability was compromised greatly by its strong self-assembling capacity. Moreover, LK7 aggregates also induced strong cytotoxicity to cells. (c) PLGA-NPs enable the capture and adsorbtion of A$\beta$42 species onto their surfaces, which reduces A$\beta$ concentrations in solution and thus slightly inhibits A$\beta$42 fibrillation without changing the cytotoxicity level. (d) LK7@PLGA-NPs enable effective interaction with A$\beta$42 to form less toxic A$\beta$-LK7@PLGA-NPs complexes, which rescues the cells from A$\beta$-induced cytotoxicity. The number of skulls indicates the level of toxic A$\beta$ aggregates.

to decrease the degradation rate of these immobilized peptides.[63]

To overcome the toxicity and poor stability issues of LK7, PLGA-NPs were used as the scaffold to conjugate LK7 to form a nanosized inhibitor, LK7@PLGA-NPs. The inhibitory effects of LK7@PLGA-NPs and its control PLGA-NPs on A$\beta$ aggregation and toxicity were carefully examined. Bare PLGA-NPs showed weak inhibitory activity toward A$\beta$ fibril formation (Figure 6a). The inhibition effect of PLGA-NPs was likely caused by adsorbing A$\beta$ species from the solution to the surface of PLGA-NPs (Figure 11c), which in turn reduced A$\beta$ concentration and its aggregation in solution. This inhibitory effect became more pronounced at higher concentrations of PLGA-NPs, consistent with previous studies.

After LK7 was conjugated onto PLGA-NPs, comparison of the inhibitory effects of LK7@PLGA-NPs and PLGA-NPs on A$\beta$ aggregation revealed some interesting similarities and differences (Figure 11d). First, both NPs were able to capture and adsorb A$\beta$ species, as demonstrated by the TEM results (Figures 6b and 7b), consistent with the previous results.[31] In addition, LK7@PLGA-NPs had a weaker negative charge than PLGA-NPs, which was attributed to the introduction of positively charged residues R and K of LK7. Since the net charges of A$\beta$42 are roughly −3 at physiological pH, the affinity between LK7@PLGA-NPs and A$\beta$42 species was further enhanced greatly, which is important to inhibit A$\beta$ aggregation and reduce its related cytotoxicity. Therefore, conjugation of


DOI: 10.1021/acsami.5b00915
ACS Appl. Mater. Interfaces 2015, 7, 5650−5662

LK7 onto PLGA-NPs made LK7@PLGA-NPs display some different inhibitory behaviors. First, LK7@PLGA-NPs exhibited better inhibitory potency than PLGA-NPs for Aβ fibril formation, especially at concentrations lower than 20 μg/mL (Figure 7a). Conversely, the same low PLGA-NPs concentration of 20 μg/mL had almost no inhibitory effect on Aβ42 aggregation (Figure 6a). Secondary, the presence of LK7@PLGA-NPs produced small amorphous Aβ species (Figure 7b), while the presence of PLGA-NPs led to some short fibrils (Figure 6b). Furthermore, LK7@PLGA-NPs partially suppressed the conformational change of Aβ from random coils to β-sheet structures, while PLGA-NPs did not (Figure 8). Third, LK7 located at the surface of PLGA-NPs would have high affinity for Aβ species (e.g., monomer, oligomer, protofibril and fibril). It is well-known that amyloid oligomers are the most toxic species generated at the early stage of amyloid aggregation.[64] Therefore, binding of LK7@PLGA-NPs to Aβ monomers and fibrils could either disrupt aggregation pathways toward the formation of toxic amyloid species or convert the existing toxic species into nontoxic ones. Alternatively, formation of Aβ-NPs complexes could also interfere with their interactions with cell membranes and membrane functions, reducing the membrane disruption effects caused by Aβ. The above three effects made LK7@PLGA-NPs possess a better inhibitory potency than PLGA-NPs (Figures 6 and 7). Another major difference is that both LK7@PLGA-NPs and PLGA-NPs displayed different inhibitory abilities to prevent Aβ-induced cytotoxicity. PLGA-NPs themselves were nontoxic to cells and they did not have influence on Aβ-induced cytotoxicity [Figures 9 and 10, and S11 and S12 (Supporting Information)]. However, LK7@PLGA-NPs protected SH-SY5Y and PC12 cells from Aβ-induced cytotoxicity in a dose-dependent manner [Figures 10 and S12 (Supporting Information)]. Therefore, collective data showed that LK7@PLGA-NPs could redirect the conformational and aggregation pathways of Aβ by converting Aβ into unstructured, amorphous, off-pathway aggregates.

Different NP-based inhibitors have been developed to prevent Aβ aggregation and toxicity.[13,34,65−68] Among them, gold NPs are the most commonly used NPs to be functionalized with peptide inhibitors for preventing Aβ aggregation, because gold NPs are readily conjugated with peptides via the gold−thiol reaction. LPFFD[26,28] and Aβ fragments[69] were reported to conjugate with gold NPs to selectively capture Aβ aggregates due to the highly affinity of these peptides for Aβ. However, gold NPs are easily aggregated into large clusters, which are likely to be accumulated in liver and spleen and cause adverse immune response.[70] Different from gold NPs, polymeric NPs, especially PLGA-NPs, possess super-biocompatibility, low toxicity, and rich functional groups, allowing conjugation with a wide variety of anti-amyloid molecules for amyloid inhibition. Song et al.[71] proposed anchoring LPFFD onto poly(N-(2-hydroxypropyl)-methacrylamide) (PHPMA) NPs, yielding LPFFD@PHPMA-NPs, which greatly suppressed Aβ fibrillogenesis, but the toxicity of the LPFFD@PHPMA-NPs was not evaluated. Skaat et al.[72] found that when conjugating polyA-ME@NPs with hydrophobic dipeptide FF, the polyA-ME@NPs slowed down Aβ aggregation but cannot completely prevent Aβ fibril formation. However, the use of PLGA-NPs as a scaffold to anchor peptide inhibitors against Aβ aggregation and toxicity has not been reported. Herein, we designed LK7 and conjugated it to PLGA-NPs, obtaining the nanosized inhibitor LK7@PLGA-NPs. We found that LK7@PLGA-NPs not only prevented the self-assembly of peptide inhibitors and the associated cytotoxicity but also greatly improved the inhibitory efficiency against Aβ aggregation and toxicity, especially at lower concentrations. In order to further enhance the inhibitory effects in vivo, our LK7@PLGA-NPs can be also functionalized with some targeted molecules (e.g., Tet-1 peptide[38,73]) for achieving specific and selective recognition of neurons. The specific targeting capacity of designed amyloid inhibitors is very important for enhancing inhibitory efficiency and reducing side effects of NPs-based inhibitors in vivo. Animal models of AD will be used to validate the inhibitory effect of LK7@PLGA-NPs in further work.

## 4. CONCLUSIONS

In this work, a peptide-functionalized nanosized inhibitor was developed to effectively prevent Aβ fibrillogenesis and toxicity. First, a novel heptapeptide inhibitor of LK7 (Ac-LVFFARK-$NH_2$) was designed by adding two positive residues, R and K, into the central hydrophobic fragment LVFFA of Aβ42. The newly added RK residues were expected to improve intermolecular interactions with Aβ via enhanced electrostatic interactions and similar conformational recognization. ThT fluorescence binding assays and TEM results confirmed that LK7 prevented Aβ42 fibrillation in a dose-dependent manner. However, LK7 was found to self-assemble into amyloid-like fibrils that led to strong cytotoxicity to cells. To address the toxicity issue of LK7, LK7 was covalently immobilized on PLGA-NPs to produce a nanosized inhibitor, LK7@PLGA-NPs. The conjugation of LK7 onto PLGA-NPs completely suppressed the self-aggregation of LK7 and thus greatly reduced the cytotoxicity caused by LK7 aggregates. Unlike the negligible inhibitory effect of pure LK7 and PLGA-NPs at the low concentrations, LK7@PLGA-NPs were not only nontoxic to cells but also greatly inhibited Aβ fibrillation and reduced Aβ-induced toxicity. Such a strong inhibitory ability of LK7@PLGA-NPs was likely attributed to several synergetic effects, including the enhancement of Aβ-LK7@PLGA-NPs interactions, the delay and disruption of conformation changes of Aβ, and the redirection of Aβ42 aggregation pathways. Finally, the working mechanisms of the inhibitory effects of LK7 and LK7@PLGA-NPs on Aβ42 aggregation were proposed based on experimental observations.

## ■ ASSOCIATED CONTENT

### Supporting Information

Figures S1−S12. This material is available free of charge via the Internet at http://pubs.acs.org.

## ■ AUTHOR INFORMATION

### Corresponding Authors

*F.-F.L.: phone, +86 22 27404981; fax, +86 22 27403389; e-mail, fufengliu@tju.edu.cn.

*Y.S.: e-mail, ysun@tju.edu.cn.

### Notes

The authors declare no competing financial interest.

## ■ ACKNOWLEDGMENTS

This work was supported by the Natural Science Foundation of China (Nos. 21376172 and 21236005) and the High-Tech Research and Development Program of China from the Ministry of Science and Technology of China (No.



DOI: 10.1021/acsami.5b00915
ACS Appl. Mater. Interfaces 2015, 7, 5650−5662

2012AA020206). J.Z. is thankful for the financial support from National Science Foundation grants (CAREER Award CBET-0952624 and CBET-1158447).

## REFERENCES

(1) Yankner, B. A.; Duffy, L. K.; Kirschner, D. A. Neurotrophic and Neurotoxic Effects of Amyloid Beta Protein: Reversal by Tachykinin Neuropeptides. *Science* **1990**, *250*, 279−282.
(2) Hardy, J.; Selkoe, D. J. The Amyloid Hypothesis of Alzheimer's Disease: Progress and Problems on the Road to Therapeutics. *Science* **2002**, *297*, 353−356.
(3) Hardy, J. Amyloid, the Presenilins and Alzheimer's Disease. *Trends Neurosci.* **1997**, *20*, 154−159.
(4) Hardy, J. A.; Higgins, G. A. Alzheimer's Disease: The Amyloid Cascade Hypothesis. *Science* **1992**, *256*, 184−185.
(5) Hawkes, C. A.; Ng, V.; Mclaurin, J. Small Molecule Inhibitors of A $\beta$-Aggregation and Neurotoxicity. *Drug Dev. Res.* **2009**, *70*, 111−124.
(6) Mangialasche, F.; Solomon, A.; Winblad, B.; Mecocci, P.; Kivipelto, M. Alzheimer's Disease: Clinical Trials and Drug Development. *Lancet Neurol.* **2010**, *9*, 702−716.
(7) Man, B. Y. W.; Chan, H. M.; Leung, C. H.; Chan, D. S. H.; Bai, L. P.; Jiang, Z. H.; Li, H. W.; Ma, D. L. Group 9 Metal-Based Inhibitors of $\beta$-Amyloid (1−40) Fibrillation As Potential Therapeutic Agents for Alzheimer's Disease. *Chem. Sci.* **2011**, *2*, 917−921.
(8) Scott, L. E.; Telpoukhovskaia, M.; Rodriguez-Rodriguez, C.; Merkel, M.; Bowen, M. L.; Page, B. D. G.; Green, D. E.; Storr, T.; Thomas, F.; Allen, D. D.; Lockman, P. R.; Patrick, B. O.; Adam, M. J.; Orvig, C. N-Aryl-Substituted 3-($\beta$-D-Glucopyranosyloxy)-2-methyl-4(1*H*)-pyridinones as Agents for Alzheimer's Therapy. *Chem. Sci.* **2011**, *2*, 642−648.
(9) Wang, Q.; Yu, X.; Patal, K.; Hu, R.; Chuang, S.; Zhang, G.; Zheng, J. Tanshinones Inhibit Amyloid Aggregation by Amyloid-$\beta$ Peptide, Disaggregate Amyloid Fibrils, and Protect Cultured Cells. *ACS Chem. Neurosci.* **2013**, *4*, 1004−1015.
(10) Du, W. J.; Guo, J. J.; Gao, M. T.; Hu, S. Q.; Dong, X. Y.; Han, Y. F.; Liu, F. F.; Jiang, S. Y.; Sun, Y. Brazilin Inhibits Amyloid $\beta$-Protein Fibrillogenesis, Remodels Amyloid Fibrils and Reduces Amyloid Cytotoxicity. *Sci. Rep.* **2015**, *5*, 7992.
(11) Funke, S. A.; Willbold, D. Peptides for Therapy and Diagnosis of Alzheimer's Disease. *Curr. Pharm. Des.* **2012**, *18*, 755−767.
(12) Watt, A. D.; Crespi, G. A.; Down, R. A.; Ascher, D. B.; Gunn, A.; Perez, K. A.; McLean, C. A.; Villemagne, V. L.; Parker, M. W.; Barnham, K. J.; Miles, L. A. Do Current Therapeutic Anti-A$\beta$ Antibodies for Alzheimer's Disease Engage the Target? *Acta Neuropathol.* **2014**, *127*, 803−810.
(13) Zhang, M.; Yu, Y.; Wang, C. X.; Yang, Y. L.; Wang, C. Nanomaterials for Reducing Amyloid Cytotoxicity. *Adv. Mater.* **2013**, *25*, 3780−3801.
(14) Wang, C.; Yang, A.; Li, X.; Li, D.; Zhang, M.; Du, H.; Li, C.; Guo, Y.; Mao, X.; Dong, M.; Besenbacher, F.; Yang, Y. Observation of Molecular Inhibition and Binding Structures of Amyloid Peptides. *Nanoscale* **2012**, *4*, 1895−1909.
(15) Tjernberg, L. O.; Naslund, J.; Lindqvist, F.; Johansson, J.; Karlstrom, A. R.; Thyberg, J.; Terenius, L.; Nordstedt, C. Arrest of $\beta$-Amyloid Fibril Formation by a Pentapeptide Ligand. *J. Biol. Chem.* **1996**, *271*, 8545−8548.
(16) Gessel, M. M.; Wu, C.; Li, H.; Bitan, G.; Shea, J. E.; Bowers, M. T. A$\beta$(39−42) Modulates A$\beta$ Oligomerization but Not Fibril Formation. *Biochemistry* **2012**, *51*, 108−117.
(17) Sahni, J. K.; Doggui, S.; Ali, J.; Baboota, S.; Dao, L.; Ramassamy, C. Neurotherapeutic Applications of Nanoparticles in Alzheimer's Disease. *J. Controlled Release* **2011**, *152*, 208−231.
(18) Li, M.; Xu, C.; Wu, L.; Ren, J.; Wang, E.; Qu, X. Self-Assembled Peptide−Polyoxometalate Hybrid Nanospheres: Two in One Enhances Targeted Inhibition of Amyloid $\beta$-Peptide Aggregation Associated with Alzheimer's Disease. *Small* **2013**, *9*, 3455−3461.
(19) Brambilla, D.; Verpillot, R.; Le Droumaguet, B.; Nicolas, J.; Taverna, M.; Kona, J.; Lettiero, B.; Hashemi, S. H.; De Kimpe, L.; Canovi, M.; Gobbi, M.; Nicolas, V.; Scheper, W.; Moghimi, S. M.; Tvaroska, I.; Couvreur, P.; Andrieux, K. PEGylated Nanoparticles Bind to and Alter Amyloid-$\beta$ Peptide Conformation: Toward Engineering of Functional Nanomedicines for Alzheimer's Disease. *ACS Nano* **2012**, *6*, 5897−5908.
(20) Cabaleiro-Lago, C.; Szczepankiewicz, O.; Linse, S. The Effect of Nanoparticles on Amyloid Aggregation Depends on the Protein Stability and Intrinsic Aggregation Rate. *Langmuir* **2012**, *28*, 1852−1857.
(21) Cabaleiro-Lago, C.; Quinlan-Pluck, F.; Lynch, I.; Lindman, S.; Minogue, A. M.; Thulin, E.; Walsh, D. M.; Dawson, K. A.; Linse, S. Inhibition of Amyloid $\beta$ Protein Fibrillation by Polymeric Nanoparticles. *J. Am. Chem. Soc.* **2008**, *130*, 15437−15443.
(22) Linse, S.; Cabaleiro-Lago, C.; Xue, W. F.; Lynch, I.; Lindman, S.; Thulin, E.; Radford, S. E.; Dawson, K. A. Nucleation of Protein Fibrillation by Nanoparticles. *Proc. Natl. Acad. Sci. U. S. A.* **2007**, *104*, 8691−8696.
(23) Li, M.; Liu, Z.; Ren, J. S.; Qu, X. G. Inhibition of Metal-Induced Amyloid Aggregation Using Light-Responsive Magnetic Nanoparticle Prochelator Conjugates. *Chem. Sci.* **2012**, *3*, 868−873.
(24) Ma, Q.; Wei, G.; Yang, X. Influence of Au Nanoparticles on the Aggregation of Amyloid-$\beta$-(25−35) Peptides. *Nanoscale* **2013**, *5*, 10397−10403.
(25) Liao, Y. H.; Chang, Y. J.; Yoshiike, Y.; Chang, Y. C.; Chen, Y. R. Negatively Charged Gold Nanoparticles Inhibit Alzheimer's Amyloid-$\beta$ Fibrillization, Induce Fibril Dissociation, and Mitigate Neurotoxicity. *Small* **2012**, *8*, 3631−3639.
(26) Olmedo, I.; Araya, E.; Sanz, F.; Medina, E.; Arbiol, J.; Toledo, P.; Alvarez-Lueje, A.; Giralt, E.; Kogan, M. J. How Changes in the Sequence of the Peptide CLPFFD-$NH_2$ Can Modify the Conjugation and Stability of Gold Nanoparticles and Their Affinity for $\beta$-Amyloid Fibrils. *Bioconjugate Chem.* **2008**, *19*, 1154−1163.
(27) Hsieh, S. C.; Chang, C. W.; Chou, H. H. Gold Nanoparticles as Amyloid-Like Fibrillogenesis Inhibitors. *Colloid Surf. B* **2013**, *112*, 525−529.
(28) Adura, C.; Guerrero, S.; Salas, E.; Medel, L.; Riveros, A.; Mena, J.; Arbiol, J.; Albericio, F.; Giralt, E.; Kogan, M. J. Stable Conjugates of Peptides with Gold Nanorods for Biomedical Applications with Reduced Effects on Cell Viability. *ACS Appl. Mater. Interfaces* **2013**, *5*, 4076−4085.
(29) Lu, T. Y.; Kao, P. F.; Lee, C. M.; Huang, S. T.; Lin, C. M. C-60 Fullerene Nanoparticle Prevents $\beta$-Amyloid Peptide Induced Cytotoxicity in Neuro 2A Cells. *J. Food Drug Anal.* **2011**, *19*, 151−158.
(30) Mahmoudi, M.; Quinlan-Pluck, F.; Monopoli, M. P.; Sheibani, S.; Vali, H.; Dawson, K. A.; Lynch, I. Influence of the Physiochemical Properties of Superparamagnetic Iron Oxide Nanoparticles on Amyloid $\beta$ Protein Fibrillation in Solution. *ACS Chem. Neurosci.* **2013**, *4*, 475−485.
(31) Cabaleiro-Lago, C.; Quinlan-Pluck, F.; Lynch, I.; Dawson, K. A.; Linse, S. Dual Effect of Amino Modified Polystyrene Nanoparticles on Amyloid $\beta$ Protein Fibrillation. *ACS Chem. Neurosci.* **2010**, *1*, 279−287.
(32) Chan, H. M.; Xiao, L.; Yeung, K. M.; Ho, S. L.; Zhao, D.; Chan, W. H.; Li, H. W. Effect of Surface-Functionalized Nanoparticles on the Elongation Phase of $\beta$-Amyloid (1−40) Fibrillogenesis. *Biomaterials* **2012**, *33*, 4443−4450.
(33) Saraiva, A. M.; Cardoso, I.; Pereira, M. C.; Coelho, M. A. N.; Saraiva, M. J.; Mohwald, H.; Brezesinski, G. Controlling Amyloid-$\beta$ Peptide(1−42) Oligomerization and Toxicity by Fluorinated Nanoparticles. *ChemBioChem* **2010**, *11*, 1905−1913.
(34) Zaman, M.; Ahmad, E.; Qadeer, A.; Rabbani, G.; Khan, R. H. Nanoparticles in Relation to Peptide and Protein Aggregation. *Int. J. Nanomed.* **2014**, *9*, 899−912.
(35) Tiwari, S. K.; Agarwal, S.; Seth, B.; Yadav, A.; Nair, S.; Bhatnagar, P.; Karmakar, M.; Kumari, M.; Chauhan, L. K.; Patel, D. K.; Srivastava, V.; Singh, D.; Gupta, S. K.; Tripathi, A.; Chaturvedi, R. K.; Gupta, K. C. Curcumin-Loaded Nanoparticles Potently Induce Adult Neurogenesis and Reverse Cognitive Deficits in Alzheimer's Disease


DOI: 10.1021/acsami.5b00915
*ACS Appl. Mater. Interfaces* 2015, 7, 5650−5662

Model via Canonical Wnt/β-Catenin Pathway. *ACS Nano* **2014**, *8*, 76−103.
(36) Mourtas, S.; Lazar, A. N.; Markoutsa, E.; Duyckaerts, C.; Antimisiaris, S. G. Multifunctional Nanoliposomes with Curcumin−Lipid Derivative and Brain Targeting Functionality with Potential Applications for Alzheimer Disease. *Eur. J. Med. Chem.* **2014**, *80*, 175−183.
(37) Palmal, S.; Maity, A. R.; Singh, B. K.; Basu, S.; Jana, N. R. Inhibition of Amyloid Fibril Growth and Dissolution of Amyloid Fibrils by Curcumin−Gold Nanoparticles. *Chemistry* **2014**, *20*, 6184−6191.
(38) Mathew, A.; Fukuda, T.; Nagaoka, Y.; Hasumura, T.; Morimoto, H.; Yoshida, Y.; Maekawa, T.; Venugopal, K.; Kumar, D. S. Curcumin Loaded-PLGA Nanoparticles Conjugated with Tet-1 Peptide for Potential Use in Alzheimer's Disease. *PLoS One* **2012**, *7*, e32616.
(39) Zhang, J.; Zhou, X.; Yu, Q.; Yang, L.; Sun, D.; Zhou, Y.; Liu, J. Epigallocatechin-3-gallate (EGCG) Stabilized Selenium Nanoparticles Coated with Tet-1 Peptide Reduce Amyloid-β Aggregation and Cytotoxicity. *ACS Appl. Mater. Interfaces* **2014**, *6*, 8475−8487.
(40) Kogan, M. J.; Bastus, N. G.; Amigo, R.; Grillo-Bosch, D.; Araya, E.; Turiel, A.; Labarta, A.; Giralt, E.; Puntes, V. F. Nanoparticle-Mediated Local and Remote Manipulation of Protein Aggregation. *Nano Lett.* **2006**, *6*, 110−115.
(41) Lazar, A. N.; Mourtas, S.; Youssef, I.; Parizot, C.; Dauphin, A.; Delatour, B.; Antimisiaris, S. G.; Duyckaerts, C. Curcumin-Conjugated Nanoliposomes with High Affinity for Aβ Deposits: Possible Applications to Alzheimer Disease. *Nanomedicine* **2013**, *9*, 712−721.
(42) Shive, M. S.; Anderson, J. M. Biodegradation and Biocompatibility of PLA and PLGA Microspheres. *Adv. Drug Delivery Rev.* **1997**, *28*, 5−24.
(43) Wang, Q.; Shah, N.; Zhao, J.; Wang, C.; Zhao, C.; Liu, L.; Li, L.; Zhou, F.; Zheng, J. Structural, Morphological, and Kinetic Studies of β-Amyloid Peptide Aggregation on Self-Assembled Monolayers. *Phys. Chem. Chem. Phys.* **2011**, *13*, 15200−15210.
(44) Zhang, N.; Chittasupho, C.; Duangrat, C.; Siahaan, T. J.; Berkland, C. PLGA Nanoparticle−Peptide Conjugate Effectively Targets Intercellular Cell-Adhesion Molecule-1. *Bioconjugate Chem.* **2008**, *19*, 145−152.
(45) Fotakis, G.; Timbrell, J. A. In Vitro Cytotoxicity Assays: Comparison of LDH, Neutral Red, MTT and Protein Assay in Hepatoma Cell Lines Following Exposure to Cadmium Chloride. *Toxicol. Lett.* **2006**, *160*, 171−177.
(46) Shearman, M. S. Toxicity of Protein Aggregates in PC12 Cells: 3-(4,5-Dimethylthiazol-2-yl)-2,5-diphenyltetrazolium Bromide Assay. *Method. Enzymol.* **1999**, *309*, 716−723.
(47) Decker, T.; Lohmannmatthes, M. L. A Quick and Simple Method for the Quantitation of Lactate-Dehydrogenase Release in Measurements of Cellular Cyto-Toxicity and Tumor Necrosis Factor (Tnf) Activity. *J. Immunol. Methods.* **1988**, *115*, 61−69.
(48) Doig, A. J. Peptide Inhibitors of β-Amyloid Aggregation. *Curr. Opin. Drug Discovery Dev.* **2007**, *10*, 533−539.
(49) Findeis, M. A.; Musso, G. M.; Arico-Muendel, C. C.; Benjamin, H. W.; Hundal, A. M.; Lee, J. J.; Chin, J.; Kelley, M.; Wakefield, J.; Hayward, N. J.; Molineaux, S. M. Modified-Peptide Inhibitors of Amyloid β-Peptide Polymerization. *Biochemistry* **1999**, *38*, 6791−6800.
(50) Takahashi, T.; Mihara, H. Peptide and Protein Mimetics Inhibiting Amyloid β-Peptide Aggregation. *Acc. Chem. Res.* **2008**, *41*, 1309−1318.
(51) Soto, C.; Kindy, M. S.; Baumann, M.; Frangione, B. Inhibition of Alzheimer's Amyloidosis by Peptides That Prevent β-Sheet Conformation. *Biochem. Biophys. Res. Commun.* **1996**, *226*, 672−680.
(52) Bodmeier, R.; Mcginity, J. W. Solvent Selection in the Preparation of Poly(DL-lactide) Microspheres Prepared by the Solvent Evaporation Method. *Int. J. Pharm.* **1988**, *43*, 179−186.
(53) Pellarin, R.; Caflisch, A. Interpreting the Aggregation Kinetics of Amyloid Peptides. *J. Mol. Biol.* **2006**, *360*, 882−892.
(54) Wahlstrom, A.; Hugonin, L.; Peralvarez-Marin, A.; Jarvet, J.; Graslund, A. Secondary Structure Conversions of Alzheimer's Aβ(1−40) Peptide Induced by Membrane-Mimicking Detergents. *FEBS J.* **2008**, *275*, 5117−5128.
(55) Panyam, J.; Labhasetwar, V. Biodegradable Nanoparticles for Drug and Gene Delivery to Cells and Tissue. *Adv. Drug Deliver. Rev.* **2003**, *55*, 329−347.
(56) Kumari, A.; Yadav, S. K.; Yadav, S. C. Biodegradable Polymeric Nanoparticles Based Drug Delivery Systems. *Colloids Surf. B* **2010**, *75*, 1−18.
(57) Wang, Q. M.; Yu, X.; Li, L. Y.; Zheng, J. Inhibition of Amyloid-β Aggregation in Alzheimer's Disease. *Curr. Pharm. Des.* **2014**, *20*, 1223−1243.
(58) Sievers, S. A.; Karanicolas, J.; Chang, H. W.; Zhao, A.; Jiang, L.; Zirafi, O.; Stevens, J. T.; Munch, J.; Baker, D.; Eisenberg, D. Structure-Based Design of Non-Natural Amino-Acid Inhibitors of Amyloid Fibril Formation. *Nature* **2011**, *475*, 96−100.
(59) Kokkoni, N.; Stott, K.; Amijee, H.; Mason, J. M.; Doig, A. J. N-Methylated Peptide Inhibitors of β-Amyloid Aggregation and Toxicity. Optimization of the Inhibitor Structure. *Biochemistry* **2006**, *45*, 9906−9918.
(60) Soto, P.; Griffin, M. A.; Shea, J. E. New Insights into the Mechanism of Alzheimer Amyloid-β Fibrillogenesis Inhibition by N-Methylated Peptides. *Biophys. J.* **2007**, *93*, 3015−3025.
(61) Taylor, M.; Moore, S.; Mayes, J.; Parkin, E.; Beeg, M.; Canovi, M.; Gobbi, M.; Mann, D. M. A.; Allsop, D. Development of a Proteolytically Stable Retro-Inverso Peptide Inhibitor of β-Amyloid Oligomerization as a Potential Novel Treatment for Alzheimer's Disease. *Biochemistry* **2010**, *49*, 3261−3272.
(62) Arai, T.; Sasaki, D.; Araya, T.; Sato, T.; Sohma, Y.; Kanai, M. A Cyclic KLVFF-Derived Peptide Aggregation Inhibitor Induces the Formation of Less-Toxic Off-Pathway Amyloid-β Oligomers. *ChemBioChem* **2014**, *15*, 2577−2583.
(63) Bilati, U.; Allemann, E.; Doelker, E. Strategic Approaches for Overcoming Peptide and Protein Instability within Biodegradable Nano- and Microparticles. *Eur. J. Pharm. Biopharm* **2005**, *59*, 375−388.
(64) Cohen, S. I.; Linse, S.; Luheshi, L. M.; Hellstrand, E.; White, D. A.; Rajah, L.; Otzen, D. E.; Vendruscolo, M.; Dobson, C. M.; Knowles, T. P. Proliferation of Amyloid-β42 Aggregates Occurs through a Secondary Nucleation Mechanism. *P. Natl. Acad. Sci. U.S.A.* **2013**, *110*, 9758−9763.
(65) Amiri, H.; Saeidi, K.; Borhani, P.; Manafirad, A.; Ghavami, M.; Zerbi, V. Alzheimer's Disease: Pathophysiology and Applications of Magnetic Nanoparticles as MRI Theranostic Agents. *ACS Chem. Neurosci.* **2013**, *4*, 1417−1429.
(66) Fazil, M.; Shadab; Baboota, S.; Sahni, J. K.; Ali, J. Nanotherapeutics for Alzheimer's Disease (AD): Past, Present and Future. *J. Drug Target.* **2012**, *20*, 97−113.
(67) Brambilla, D.; Le Droumaguet, B.; Nicolas, J.; Hashemi, S. H.; Wu, L. P.; Moghimi, S. M.; Couvreur, P.; Andrieux, K. Nanotechnologies for Alzheimer's Disease: Diagnosis, Therapy, and Safety Issues. *Nanomedicine* **2011**, *7*, 521−540.
(68) Pehlivan, S. B. Nanotechnology-Based Drug Delivery Systems for Targeting, Imaging and Diagnosis of Neurodegenerative Diseases. *Pharm. Res.* **2013**, *30*, 2499−2511.
(69) Triulzi, R. C.; Dai, Q.; Zou, J. H.; Leblanc, R. M.; Gu, Q.; Orbulescu, J.; Huo, Q. Photothermal Ablation of Amyloid Aggregates by Gold Nanoparticles. *Colloid Surf. B* **2008**, *63*, 200−208.
(70) Zhang, X. D.; Wu, D.; Shen, X.; Liu, P. X.; Fan, F. Y.; Fan, S. J. In Vivo Renal Clearance, Biodistribution, Toxicity of Gold Nanoclusters. *Biomaterials* **2012**, *33*, 4628−4638.
(71) Song, Y.; Cheng, P. N.; Zhu, L.; Moore, E. G.; Moore, J. S. Multivalent Macromolecules Redirect Nucleation-Dependent Fibrillar Assembly into Discrete Nanostructures. *J. Am. Chem. Soc.* **2014**, *136*, 5233−5236.
(72) Skaat, H.; Chen, R.; Grinberg, I.; Margel, S. Engineered Polymer Nanoparticles Containing Hydrophobic Dipeptide for Inhibition of Amyloid-β Fibrillation. *Biomacromolecules* **2012**, *13*, 2662−2670.
(73) Zhang, J. N.; Zhou, X. B.; Yu, Q. Q.; Yang, L. C.; Sun, D. D.; Zhou, Y. H.; Liu, J. Epigallocatechin-3-gallate (EGCG)-Stabilized Selenium Nanoparticles Coated with Tet-1 Peptide To Reduce


DOI: 10.1021/acsami.5b00915
*ACS Appl. Mater. Interfaces* 2015, 7, 5650−5662

Amyloid-$\beta$ Aggregation and Cytotoxicity. *ACS Appl. Mater. Interfaces* **2014**, *6*, 8475−8487.



DOI: 10.1021/acsami.5b00915
*ACS Appl. Mater. Interfaces* 2015, 7, 5650−5662